Temporal oscillations in the simulation of foam enhanced oil recovery

van der Meer, Jakolien; Kraaijevanger, JFBM; Möller, Matthias; Jansen, Jan Dirk

DOI
10.3997/2214-4609.201601850

Publication date
2016

Document Version
Final published version

Published in
Proceedings of the 15th European Conference on the Mathematics of Oil Recovery

EAGE

ECMOR XV

Th Efe 07

Temporal oscillations in the simulation of foam enhanced oil recovery

J.M. van der Meer* (Delft University of Technology), J.B.F.M. Kraaijevanger (Shell Global Solutions), M. Möller (Delft University of Technology) & J.D. Jansen (Delft University of Technology)

SUMMARY

Many enhanced oil recovery (EOR) processes can be described using partial differential equations with parameters that are strongly non-linear functions of one or more of the state variables. Typically these non-linearities result in solution components changing several orders of magnitude over small spatial or temporal distances. The numerical simulation of such processes with the aid of finite volume or finite element techniques poses challenges. In particular, temporally oscillating state variable values are observed for realistic grid sizes when conventional discretization schemes are used. These oscillations, which do not represent a physical process but are discretization artifacts, hamper the use of the forward simulation model for optimization purposes. To analyze these problems, we study the dynamics of a simple foam model describing the interaction of water, gas and surfactants in a porous medium. It contains sharp gradients due to the formation of foam. The simplicity of the model allows us to gain a better understanding of the underlying processes and difficulties of the problem. The foam equations are discretized by a first-order finite volume method. Instead of using a finite volume method with a standard interpolation procedure, we opt for an integral average, which smooths out the discontinuity caused by foam generation. We introduce this method by applying it to the heat equation with discontinuous thermal conductivity. A similar technique is then applied to the foam model, reducing the oscillations drastically, but not removing them.

Introduction

Foam was first applied in the oil industry in the late 1950s to decrease gas mobility and hence reduce the undesirable effect of viscous fingering and gravity override in subsurface porous media flow (Fried, 1961). To generate foam in a subsurface oil reservoir, usually a mixture of chemicals and water is injected into the reservoir, which together with the injected gas forms a foam. These chemicals make a large contribution to the production costs, and therefore the goal is to minimize their amount. To determine the required amount of chemicals for an economically profitable production level, reliable simulations are needed (van der Meer et al., 2014).
The generation of foam can be described by a system of partial differential equations with strongly non-linear functions, which impose challenges for the numerical modeling. Former studies by Namdar Zanganeh et al. (2014), Ashoori et al. (2011) and Ashoori et al. (2012) show the occurrence of temporally strongly oscillating solutions when using forward simulation models, that are entirely due to discretization artifacts (Fig. 1).
To analyze these problems, we study the dynamics of a one-dimensional, two-phase incompressible foam model, based on the Buckley-Leverett equation (Buckley and Leverett, 1942). In this simplified model we consider a one-dimensional horizontal reservoir with one injection and one production well. Gas is injected in the reservoir, which consists of a porous medium filled with a mixture of water and surfactants (to simplify the model, oil is assumed to be absent). As soon as the injected gas comes into contact with a sufficient amount of water and surfactant a foam is generated. The foam will cause a rapid decrease of the gas mobility, because it captures the gas in bubbles that are separated by liquid films (lamellae) between the pore walls (Rossen, 2013). The water mobility is not influenced by foam in these models and hence the mobility ratio between gas and water is reduced. This will increase the time that the injected gas needs to reach the production well (breakthrough time).
The governing equations of the foam model are solved sequentially in time by the implicit pressure explicit saturation (IMPES) method (Aziz and Settari, 1979). In space the saturation equation is solved by a second-order MUSCL scheme (van Leer, 1979), and in time by the second-order semi-implicit trapezoidal method. The pressure equation is discretized in space by a first-order finite volume method, and the resulting linear system is solved by the Cholesky method (van der Meer et al., 2014). Instead of using a standard interpolation procedure for the phase mobilities when discretizing the pressure equation, we opt for an integral average. The highly non-linear transition caused by the generation of foam is hence integrated over a range of saturation values between two neighboring grid blocks, reducing jumps in the solution.
We first introduce this method by applying it to the heat equation with discontinuous thermal conductivity. The initially strongly oscillating solution becomes monotonic by introducing this small change in the discretization scheme. A similar technique is then applied to the foam model, reducing the oscillations drastically, but not removing them entirely. We analyze this difference in behavior by performing a continuity analysis of the numerical scheme for each model. Furthermore, we illustrate the effectiveness of our numerical scheme by comparing it with other finite volume schemes, which vary in order, interpolation procedure and the amount of artificial diffusion.

Mathematical model

Conservation law

We study the one-dimensional foam model defined in van der Meer et al. (2014). In case of an incompressible fluid in a porous medium, mass conservation of the phase saturation $S_\alpha \in [0,1]$ is given by

$$\phi \partial_t S_\alpha = -\partial_x (f_\alpha u), \quad \forall x \in [0,1], t \geq 0, \tag{1}$$

where the subscript $\alpha \in \{w,g\}$ denotes the water or gas phase, ϕ is the reservoir porosity, $f_\alpha = \lambda_\alpha / \lambda$ is the phase fractional flow function, and u is the total Darcy velocity which follows from Darcy's law,

$$u = -\lambda \partial_x p. \tag{2}$$

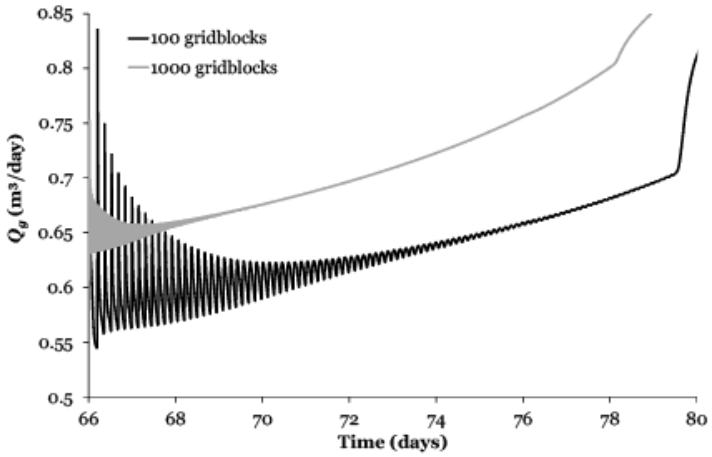

Figure 1 *Temporal oscillations in the injection rate due to generation of foam, that are highly dependent on the grid resolution (Namdar Zanganeh et al., 2014).*

Here p is the reservoir pressure, and λ is the total mobility, which is given by the sum of the phase mobilities as

$$\lambda_\alpha = k\frac{k_{r\alpha}(S_\alpha)}{\mu_\alpha}, \tag{3}$$

where k is the absolute permeability, μ_α the phase viscosity and $k_{r\alpha}$ the phase relative permeability, defined by the Brooks-Corey model (Brooks and Corey, 1964). The Brooks-Corey relative permeability functions for gas and water are given by

$$k_{rw} = k_{rwe}\left(\frac{S_w - S_{wc}}{1 - S_{wc} - S_{gr}}\right)^{n_w}, \quad k_{rg} = k_{rge}\left(\frac{S_g - S_{gr}}{1 - S_{wc} - S_{gr}}\right)^{n_g}, \tag{4}$$

where k_{rwe} and k_{rge} are the endpoint relative permeabilities, S_{wc} is the connate water saturation, S_{gr} is the residual gas saturation and n_w and n_g are power coefficients, which all depend on the specific interface properties of the rock and the fluids. From the definition of saturation it follows that the sum of the phase saturations is one everywhere, i.e.

$$\sum_\alpha S_\alpha = 1, \text{ with } \alpha \in \{w, g\}, \tag{5}$$

so that we only have to solve for one phase. Hence, Eq. (1), (2) and (5) imply that

$$\partial_x u = \partial_x(-\lambda\,\partial_x p) = 0, \quad \Rightarrow u(x,t) = \overline{u}(t), \tag{6}$$

which describes the pressure decay in the porous medium.

Foam model

If gas comes into contact with a sufficient amount of water and surfactants a foam will form. This will cause a rapid decrease in the gas mobility λ_g, which can be modeled by decreasing the relative gas permeability function by a mobility reduction factor f_{mr}

$$k_{rg} := \frac{k^o_{rg}}{f_{mr}}, \quad f_{mr} = 1 + R \cdot F_w \cdot F_s, \tag{7}$$

where k^o_{rg} is the relative permeability of the gas in its original state using the Brooks-Corey model, R is a constant that accounts for the maximum flow resistance of the foam, and F_w and F_s are functions that describe the sensitivity of the foam to water saturation and surfactant concentration, respectively (Boeije

and Rossen, 2013). We assume that the surfactant concentration is the same everywhere, so that $F_s = 1$. Because foam forms almost instantly, F_w is modeled by the Heaviside step function

$$F_w = H(S_w - S_w^*), \tag{8}$$

where S_w^* is the least amount of water that is needed to form a foam. Since a sudden jump in the mobility of the gas at S_w^* will lead to discontinuous derivatives in the simulator, this jump is approximated by a continuous arctangent function, so that it is smeared over a width that scales with $1/\kappa$

$$F_w = 0.5 + \frac{\arctan\left(\kappa(S_w - S_w^*)\right)}{\pi}, \tag{9}$$

where κ is a positive parameter that controls the width of the gas-foam transition. In Fig. 2 the relative permeability function described here is shown. The flux function and its derivative for the scaled parameters are shown in Fig. 3.

Non-dimensional formulation

To reduce the number of parameters we scale the model given by Eq. (1), (2) and (6), in a similar way as done by Riaz and Tchelepi (2007). If we let L be a characteristic length scale of the model, and U a characteristic velocity scale we can scale the variables as follows

$$\begin{aligned}
x &= Lx^*, && (10)\\
\partial_x &= \frac{\partial_{x^*}}{L}, && (11)\\
u &= Uu^*, && (12)\\
t &= \frac{\phi L(1 - S_{wc} - S_{gr})}{U} t^*, && (13)\\
p &= \frac{\mu UL}{k} p^*, && (14)
\end{aligned}$$

where the asterisk denotes a non-dimensional variable. The relative permeability functions are scaled by their endpoint relative permeabilities, i.e. the relative permeability of the residual water and gas saturation, $k_{rwe} = k_{rw}(S_{gr})$ and $k_{rge} = k_{rg}(1 - S_{wc})$, respectively. The gas saturation is normalized by $S_g^* = \frac{(S_g - S_{gr})}{(1 - S_{wc} - S_{gr})}$. Substituting these variables into the dimensional model leads to a non-dimensional system of the form

$$\begin{aligned}
\partial_{t^*} S_g^* &= -\partial_{x^*}\left(\frac{k_{rg}^* M}{\lambda^*} u^*\right), && (15)\\
u^* &= -\lambda^* \partial_{x^*} p^*, && (16)\\
\partial_{x^*} u^* &= 0, && (17)
\end{aligned}$$

where $\lambda^* = Mk_{rg}^* + k_{rw}^*$ is the dimensionless mobility function. Here, the variable M denotes the dimensionless mobility ratio, given by

$$M = \frac{\mu_w}{\mu_g} \frac{k_{rge}}{k_{rwe}}. \tag{18}$$

The mobility ratio together with the dimensionless foam parameters R, κ and S_w^*, dimensionless injection rate I^* and porosity ϕ, determine the entire behavior of the fluids for a certain initial boundary value problem. In the rest of the article we will drop the asterisk for readability and define $S \equiv S_g$ and $f \equiv \frac{k_{rg} M}{\lambda}$. Together with initial and boundary conditions we then have the following initial boundary-value prob-

lem,

$$\begin{aligned}
\partial_t S &= -\partial_x (fu), && \forall x \in [0,1], t \geq 0, && (19)\\
\partial_x u &= 0, && \forall x \in [0,1], && (20)\\
u &= -\lambda \partial_x p, && \forall x \in [0,1], && (21)\\
S(x,0) &= 0, && \forall x \in [0,1], && (22)\\
S(0,t) &= 1, && \forall t \geq 0, && (23)\\
u(0,t) &= u_L, && \forall t \geq 0, && (24)\\
p(1,t) &= p_R, && \forall t \geq 0, && (25)
\end{aligned}$$

where we fix the velocity on the left boundary and the pressure on the right boundary. Due to the incompressibility condition, the velocity will now be constant in time and space. Hence, the solution of Eq. (19) is independent of Eq. (20) and the system is only weakly coupled through the total mobility. Later in this paper we will also investigate the strongly coupled system, where the pressure is fixed on both sides of the domain (i.e. Eq. (24) is replaced by $p(0,t) = p_L$).

Numerical oscillations

We solve the foam model numerically for multiple sets of foam parameters, where we use the IMPES method with a second-order MUSCL solver for the explicit part. A necessary condition for stability of the saturation update, is given by the Courant-Friedrichs-Lewy (CFL) condition. Due to the high wave speeds around the critical water saturation, as shown in Fig. 3b, the time step can become extremely restricted if κ is increased. In Fig. 4 the saturation profile of the foam model for one parameter set is shown, which is stable in both space and time. However, if we take a look at the pressure solutions in Fig. 4 we see that the pressure solution is oscillating in time. In Fig. 5 we show that the amplitude of the oscillations is highly dependent on the value of the foam parameters R and κ. Both increasing the foam resistance R and the steepness of the foam transition κ will cause stronger oscillatory behavior. Both the amplitude and frequency of the oscillations seem directly related to the grid size. Decreasing the grid size will decrease the amplitude of the oscillations, and increase its frequency, as depicted in Fig. 1. Moreover, we can connect each oscillation to a grid block the shock has passed as shown in Fig. 6, which was also observed by Namdar Zanganeh et al. (2014). So unless the step size is drastically reduced, the oscillations will not disappear by using a higher resolution in space (Fig. 7). Considering the already small time step size due to the CFL condition, it is not feasible to reduce the step size by a large amount.

Heat equation with discontinuous conductivity

Similar oscillations in time were observed for the one-dimensional heat equation with a discontinuous coefficient, defined by

$$\begin{aligned}
\partial_t T &= -\partial_x q, && \forall x \in [0,1], t \geq 0, && (26)\\
q &= -a(T)\partial_x T, && && (27)\\
T(x,0) &= 0, && \forall x \in [0,1], && (28)\\
T(0,t) &= 1, && \forall t \geq 0, && (29)\\
T(1,t) &= 0, && \forall t \geq 0, && (30)\\
& && && (31)
\end{aligned}$$

where T is the temperature and a the thermal conductivity given by a step function,

$$a(T) := \begin{cases} \varepsilon & \text{if } T \leq T^*, \\ 1 & \text{if } T > T^*, \end{cases} \qquad (32)$$

as depicted in Fig. 8. We semi-discretize this equation with the finite volume method over a finite

interval $[0,1]$ that is divided into N grid cells with size $\Delta x = 1/N$ as shown in Fig. 9, where $x_i = i\Delta x$ denotes the midpoint of the i-th grid cell and $T_i = T(x_i)$ the average temperature in the i-th grid cell. The cell centers are indexed by $i \in \{0,\dots,N\}$ and the cell interfaces by $i \in \{-\frac{1}{2},\frac{1}{2},\dots,N+\frac{1}{2}\}$. Hence, we obtain an ordinary differential equation for T_i,

$$\dot{T}_i = \frac{q_{i-\frac{1}{2}} - q_{i+\frac{1}{2}}}{\Delta x}, \qquad \forall i \in \{0,\dots,N\}, \tag{33}$$

$$q_{i+\frac{1}{2}} = -a_{i+\frac{1}{2}} \frac{T_{i+1} - T_i}{\Delta x}, \qquad \forall i \in \{0,\dots,N-1\}, \tag{34}$$

$$q_{-\frac{1}{2}} = -a(T_0) \frac{T_0 - T_L}{\Delta x/2}, \tag{35}$$

$$q_{N+\frac{1}{2}} = -a(T_N) \frac{T_R - T_N}{\Delta x/2}, \tag{36}$$

where $\dot{T}_i$ is the time derivative of T_i, and $a_{i+\frac{1}{2}}$ is the approximation of the thermal conductivity on the cell interface, which can be computed by one of the following approaches

- upwind: $a_{i+\frac{1}{2}} = \begin{cases} a(T_i), & \text{if } T_i \geq T_{i+1}, \\ a(T_{i+1}), & \text{if } T_i < T_{i+1}, \end{cases}$
- harmonic average: $a_{i+\frac{1}{2}} = \frac{2a(T_i)a(T_{i+1})}{a(T_i)+a(T_{i+1})}$,
- arithmetic average: $a_{i+\frac{1}{2}} = \frac{1}{2}(a(T_i) + a(T_{i+1}))$,
- maximum average: $a_{i+\frac{1}{2}} = \max\{a(T_i), a(T_{i+1})\}$.

Because the temperature decreases from left to right, the maximum average is identical to the upwind average for this problem, and the harmonic average is unsuitable since it converges very slowly if ε is small. Eq. 33 is then solved by the forward Euler method for the other two averaging procedures and a constant time step $\Delta t = 1.8 \cdot 10^{-4}$, which satisfies the CFL criterium.

Temporal oscillations

Independent of the choice of the flux discretization, this will lead to oscillatory behavior in time, as shown in Fig. 10b and 10d. As a remedy we take the integral over the discontinuous parameter a, defined by

$$A(T) \equiv \int_0^T a(v)dv, \tag{37}$$

so that the solution of the PDE satisfies

$$q = -a(T)\partial_x T = -\frac{\partial A}{\partial x}. \tag{38}$$

This suggests the following choice for the numerical flux,

$$q_{i+\frac{1}{2}} = \frac{A(T_i) - A(T_{i+1})}{\Delta x} = -\frac{1}{\Delta x}\int_{T_i}^{T_{i+1}} a(v)dv, \tag{39}$$

which corresponds to the choice

$$a_{i+\frac{1}{2}} = \frac{A(T_{i+1}) - A(T_i)}{T_{i+1} - T_i} = \frac{1}{T_{i+1} - T_i} \int_{T_i}^{T_{i+1}} a(v)dv. \tag{40}$$

If this integral is approximated using the Trapezoidal rule, it will reduce to the arithmetic average discretization, leading to non-physical oscillations. However, if we evaluate the integral exactly, $A(T)$ becomes a C^0-continuous function of the temperature. Hence the flux q will be a continuous function of the temperature. From Eq. (33) it then follows that $\dot{T}$ is a C^0-continuous function and so the solution for T is C^1-continuous (Coddington and Levinson, 1955). In Fig. 10f the solution in time using the integral average (40) is depicted. The resulting temperature is monotone in time, but exhibits a stepwise increase that will damp out after some time. Also note that the integral average approaches the exact solution most closely among the three methods. Of all cases the upwind average performs worst.

In order to determine the nature of the oscillations we analyze the (almost) semi-discrete behavior of the equation by taking a very small time step. The results are shown in Fig. 11 and 12. The integral average method does not show any improvement by decreasing the time step, since the stepwise behavior is still visible. The smoothness of the solution using the other two averaging methods improves significantly by taking a smaller time step, since the amplitude of the oscillations is smaller and the oscillations are mainly restricted to a small time interval occurring after the shock wave has passed. Behind the shock front the solutions show some low-frequency oscillations, with a decreasing amplitude, that resemble the stepwise pattern we observed for the integral average method. The integral average is thus able to remove the high-frequency oscillations, but not enough to get rid of the low-frequency oscillations.

Let us examine the time interval where the high frequency oscillations occur for the first two averaging methods. The length of this interval seems to be dependent on the grid resolution and it reduces if the grid is refined. As the time step is reduced the oscillations decrease in amplitude, and finally a constant state is reached, which approaches the temperature at which the heat conductivity is discontinuous. The length of this time interval corresponds to the time that the numerical shock precedes the analytical shock. If the integral average is applied no such constant state is obtained and the numerical shock fits the analytical shock quite well.

Foam model with discontinuous mobility

If we consider the foam model given by Eq. (19) to (24), we observe many similarities with the heat equation with discontinuous conductivity. The system contains a discontinuous parameter λ, shown in Fig. 13. Like the thermal conductivity a, this parameter λ is responsible for the time oscillations that were observed in the pressure solution.

Finite volume scheme using integral average

If we discretize the system of equations with the finite volume method we obtain the following semi-discrete system in x_i

$$\dot{S}_i = -\overline{u}\frac{f_{i+\frac{1}{2}} - f_{i-\frac{1}{2}}}{\Delta x}, \qquad \text{for } i \in \{0,\ldots,N\}, \tag{41}$$

$$\partial_x \overline{u}_i = \frac{\overline{u}_{i+\frac{1}{2}} - \overline{u}_{i-\frac{1}{2}}}{\Delta x} = 0, \qquad \text{for } i \in \{0,\ldots,N\}, \tag{42}$$

$$\overline{u}_{i+\frac{1}{2}} = -\lambda_{i+\frac{1}{2}}\frac{p_{i+1} - p_i}{\Delta x}, \qquad \text{for } i \in \{0,\ldots,N-1\}, \tag{43}$$

$$\overline{u}_{-\frac{1}{2}} = -\lambda(S_0)\frac{p_0 - p_L}{\Delta x/2}, \tag{44}$$

$$\overline{u}_{N+\frac{1}{2}} = -\lambda(S_N)\frac{p_R - p_N}{\Delta x/2}, \tag{45}$$

where $\lambda_{i+\frac{1}{2}}$ is approximated on the cell interface by one of the following interpolation methods

- upwind: $\lambda_{i+\frac{1}{2}} = \begin{cases} \lambda(S_i), & \text{if } u_i > 0, \\ \lambda(S_{i+1}), & \text{if } u_i < 0, \end{cases}$

- harmonic average: $\lambda_{i+\frac{1}{2}} = \frac{2\lambda(S_i)\lambda(S_{i+1})}{\lambda(S_i)+\lambda(S_{i+1})}$,

- arithmetic average: $\lambda_{i+\frac{1}{2}} = \frac{1}{2}(\lambda(S_i)+\lambda(S_{i+1}))$,

- maximum: $\lambda_{i+\frac{1}{2}} = \max(\lambda(S_i), \lambda(S_{i+1}))$.

It was shown earlier, that this approach leads to non-physical oscillations in time. The amplitude of these oscillations depends, besides the foam parameters and the grid size, on the adopted interpolation method. The upwind average will cause similar oscillations as the harmonic average applied to the finite volume discretization of the foam model. The mean average method suffers much less from oscillations than the harmonic average method. It is reasonable to assume that if we choose this average in a smarter way, it will be possible to reduce the oscillations even further.

Starting from Eq. (2) and (6) with $\overline{u}(t) = 1$, it follows that

$$p(x,t) = \int_x^1 \frac{dx}{\lambda(S(x,t))} + p_R, \tag{46}$$

A central two-point discretization for the spatial derivative leads to the semi-discrete equation for the pressure as a function of time only

$$p_i(t) = \Delta x \sum_{j=i}^{N} \frac{1}{\lambda(S_j(t), S_{j+1}(t))} + p_R. \tag{47}$$

Hence p is a smooth function of time if $\frac{1}{\lambda(S_i,S_{i+1})}$ and $\overline{u}(t)$ are smooth. If we fix the velocity at the left boundary, it will be constant in time and space, due to the incompressibility condition. This means we only have to obtain a smooth formulation for the sum over the mobilities in time. In order to achieve this we take the cell-integral average of $\frac{1}{\lambda}$ over the interval $[S_i, S_{i+1}]$, given by

$$\frac{1}{\lambda(S_j, S_{j+1})} = \frac{1}{S_{i+1} - S_i} \int_{S_i}^{S_{i+1}} \frac{1}{\lambda(S)} dS, \tag{48}$$

so that

$$\lambda_{i+\frac{1}{2}} = \frac{S_{i+1} - S_i}{\int_{S_i}^{S_{i+1}} \frac{1}{\lambda(S)} dS}. \tag{49}$$

Alternatively, we can take the integral over λ directly, so that

$$\lambda_{i+\frac{1}{2}} = \frac{1}{S_{i+1} - S_i} \int_{S_i}^{S_{i+1}} \lambda(S) dS. \tag{50}$$

If λ is a smooth function of S and $\Delta S_i = |S_{i+1} - S_i|$ is small, the integral averages are similar to standard averages like the arithmetic average. It can be shown that in this case

$$\frac{1}{S_{i+1} - S_i} \int_{S_i}^{S_{i+1}} \lambda(S) dS = \frac{\lambda(S_i) + \lambda(S_{i+1})}{2} + \mathcal{O}((\Delta S_i)^2). \tag{51}$$

Finally, to avoid very large contributions to the sum of inverse mobilities $\frac{1}{\lambda(S_i,S_{i+1})}$, we could opt for another 'averaging method', given by

$$\lambda_{i+\frac{1}{2}} = \max\{\lambda(S_i), \lambda(S_{i+1})\}. \tag{52}$$

We solve the system given by Eq. (15) to (17) with the IMPES method, where we make use of different averaging methods for the total mobility. The resulting pressure solutions in time are shown in Fig. 14 for a grid resolution $N = 100$.

From these results it is clear that the integral average is not sufficient to remove the oscillations, although the amplitude is halved compared to the upwind and harmonic average. However, if we use a coarser grid with resolution $N = 10$, the oscillations are more pronounced, and it becomes apparent that the integral average has a smoothing effect on the oscillations (Fig. 15). There are several things worth noting in Fig. 15. First, the number of oscillations is the same for all averaging methods and matches the number of grid blocks behind the saturation front. Furthermore, note that the amplitude of the oscillations differs drastically, with approximately a factor five between the upwind average and the maximum average (Fig. 16). Besides that, the nature of the discontinuity varies for the different averaging methods. It can be seen that for the maximum mobility the oscillations are saw tooths, also called removable discontinuities, since the limit on both sides is equal. These discontinuities are not continuously differentiable and hence are C^0-continuous functions. The integral average, on the contrary, is continuously differentiable.

Discussion and Conclusion

We studied two types of temporal oscillations, that are entirely due to the grid discretization. The first type of oscillations appear in the parabolic heat equation with discontinuous conductivity, when discretized with the finite volume method. The second type of oscillations are found in the elliptic part of a two-phase, incompressible foam model, with (almost) discontinuous mobility. To get rid of these non-physical oscillations we changed the averaging method on the grid interfaces of the finite volume scheme. Instead of taking an average of the conductivity/mobility on each side of the grid interface, all (unknown) values in between are taken into account, by integrating the conductivity/mobility over the given temperature/saturation range. This can be seen as a sort of flux correction method, where linear interpolation is used to approximate the in-between values. Applying the integral average to the non-linear heat equation with discontinuous heat conductivity removes the oscillations for our test cases. Applying the same scheme to the foam model, does not solve the numerical problems. However, integration over the mobility does change the nature of the discontinuities. The pressure solution becomes continuously differentiable in time, and the amplitude of the oscillations is reduced by a significant amount. Still, the maximum average performs best, when we compare the different averaging schemes for all test cases.

Acknowledgements

This research was carried out within the context of the Recovery Factory project at TU Delft, sponsored by Shell Global Solutions International. The first author would like to thank Bill Rossen of Delft University of Technology for useful discussions about the modeling of foam.

References

Ashoori, E., Marchesin, D. and Rossen, W.R. [2011] Roles of transient and local equilibrium foam behavior in porous media: Traveling wave. *Colloids and Surfaces A: Physicochemical and Engineering Aspects*, **377**(1-3), 228–242.

Ashoori, E., Marchesin, D. and Rossen, W.R. [2012] Stability Analysis of Uniform Equilibrium Foam States for EOR Processes. *Transport in Porous Media*, **92**(3), 573–595.

Aziz, K. and Settari, A. [1979] *Petroleum reservoir simulation*. Chapman & Hall.

Boeije, C.S. and Rossen, W.R. [2013] Fitting Foam Simulation Model Parameters for SAG Foam Applications. In: *SPE Enhanced Oil Recovery Conference*. Society of Petroleum Engineers.

Brooks, R. and Corey, T. [1964] Hydraulic properties of porous media. Tech. rep., Colorado State University, Fort Collins, Colorado.

Buckley, S.E. and Leverett, M.C. [1942] Mechanism of fluid displacements in sands. *Transactions of the AIME*, **146**, 107–116.

Coddington, E.A. and Levinson, N. [1955] *Theory of ordinary differential equations*. McGraw-Hil.

Fried, A.N. [1961] United States Bureau of Mines Bulletin 5866. Tech. rep., Bureau of Mines.

van Leer, B. [1979] Towards the Ultimate Conservative Difference Scheme. V. A Second-Order Sequel to Godunov's Method. *Journal of Computational Physics*, **32**(1), 101 – 136.

van der Meer, J., van Odyck, D., Wirnsberger, P. and Jansen, J.D. [2014] High-order Simulation of Foam Enhanced Oil Recovery. In: *ECMOR 2014*. 8–11.

Namdar Zanganeh, M., Kraaijevanger, J., Buurman, H.W., Jansen, J.D., Rossen, W.R. and Zanganeh, M.N. [2014] Challenges in adjoint-based optimization of a foam EOR process. *Computational Geosciences*, **18**(3-4), 563–577.

Riaz, A. and Tchelepi, H.A. [2007] Stability of two-phase vertical flow in homogeneous porous media. *Physics of Fluids*, **19**(7).

Rossen, W.R. [2013] Numerical Challenges in Foam Simulation : A Review. In: *SPE Annual Technical Conference and Exhibition held in New Orleans*. SPE International, New Orleans.

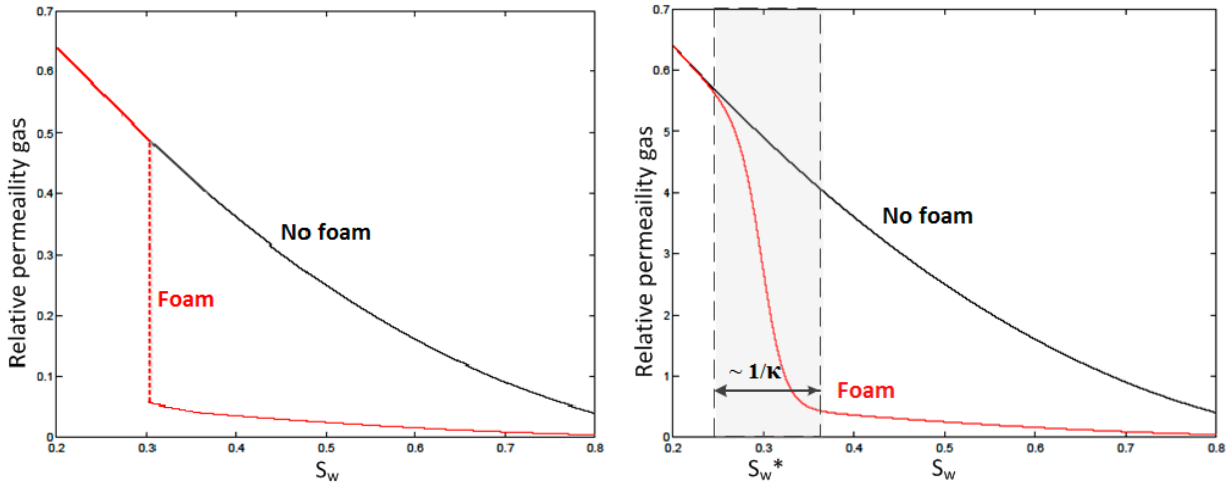

(a) $\kappa = \infty$ (b) $\kappa = 40$

Figure 2 *Relative permeability function for the model with and without foam. The sudden transition due to foam in the left figure given by Eq. (7) and (8) is approximated in the right figure by a continuous line given by Eq. (7) and (9), where* $S^* = 0.3$, $\kappa = 40$, $R = 10$ *and* $M = 1$.

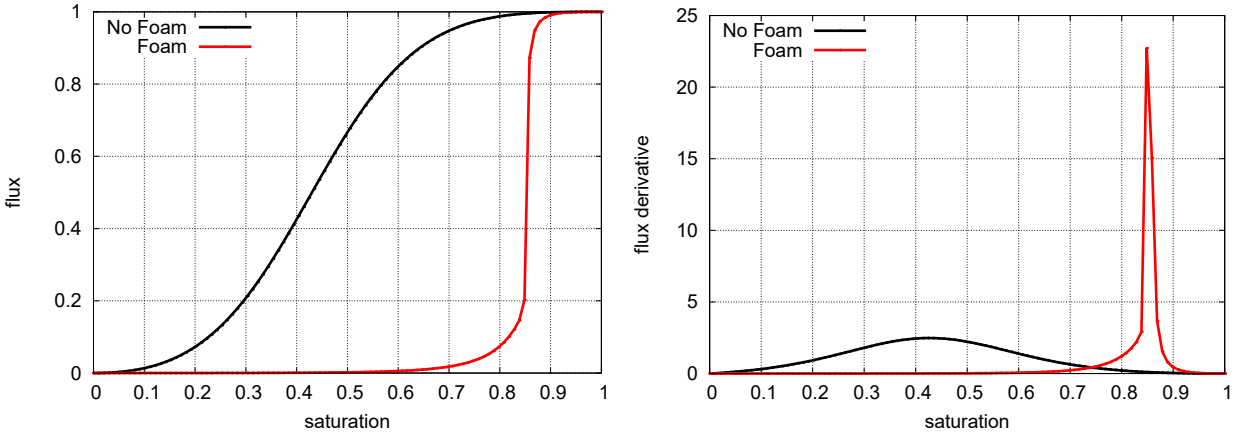

(a) flux (b) flux derivative

Figure 3 *Flux function and derivative for the model with and without foam, where* $S_w^* = 0.15$, $\kappa = 1000$, $R = 1000$ *and* $M = 10$.

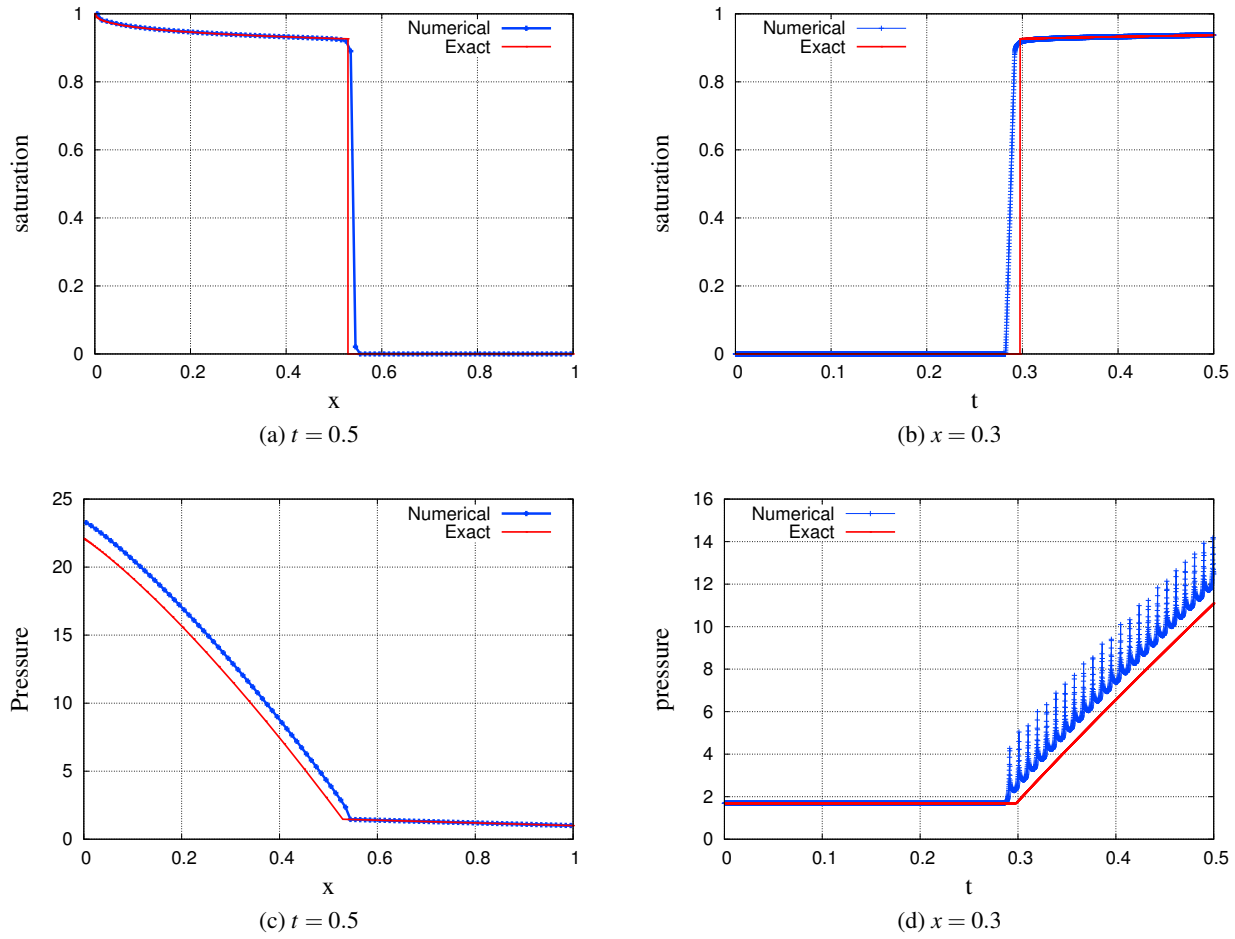

(a) $t = 0.5$ (b) $x = 0.3$

(c) $t = 0.5$ (d) $x = 0.3$

Figure 4 *Numerical and analytical saturation and pressure profiles of the foam model with resolution N = 100 and M = 1, $S^*_w = 0.15$, $\kappa = 1000$ and R = 10000, $u_L = 1$, $p_R = 1$.*

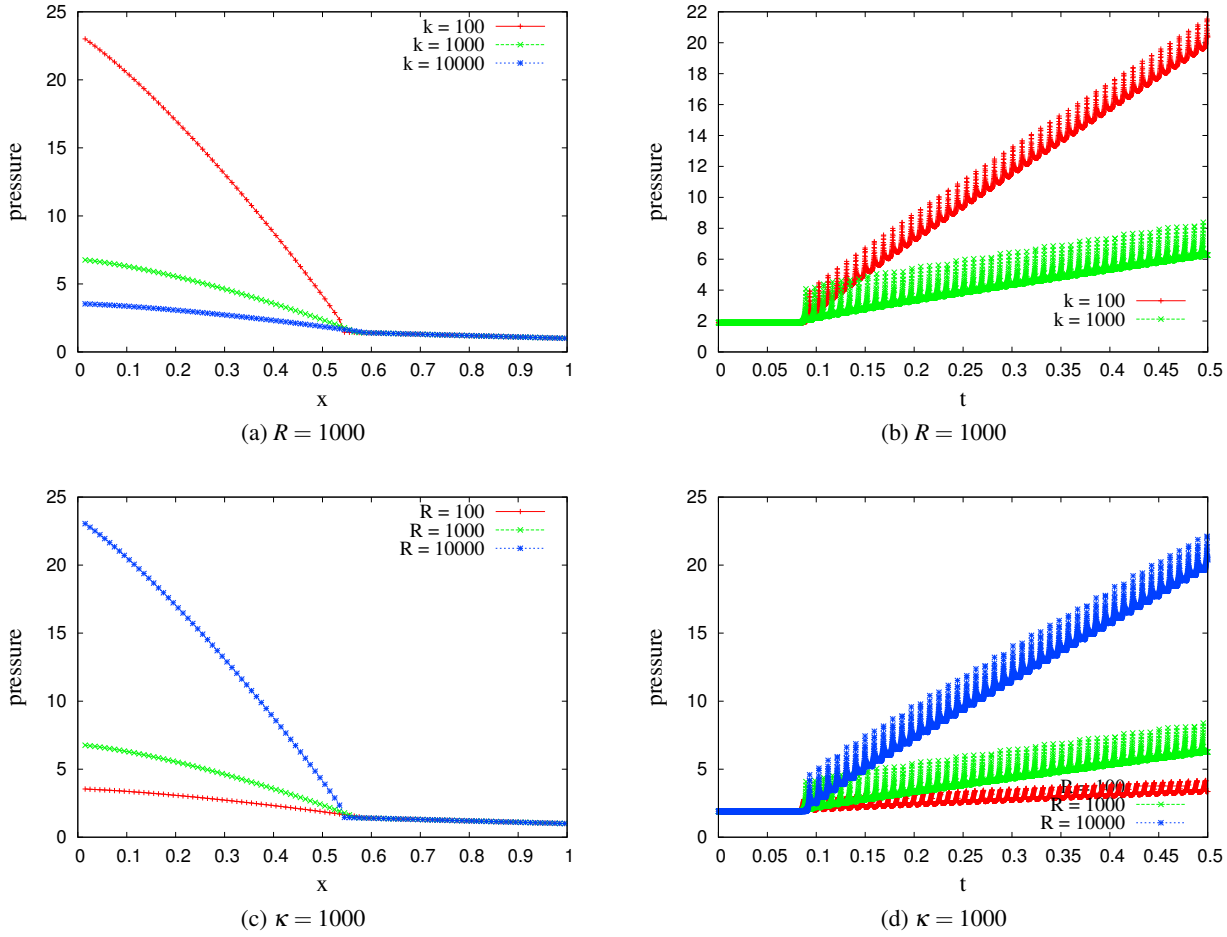

(a) $R = 1000$ (b) $R = 1000$

(c) $\kappa = 1000$ (d) $\kappa = 1000$

Figure 5 *(Left) pressure versus spatial coordinate at $t = 0.1$, (Right) pressure versus time at $x = 0.5$, of the foam model with resolution $N = 100$ and $M = 1$, $S^*_w = 0.2$, $p_L = 11$, $p_R = 1$.*

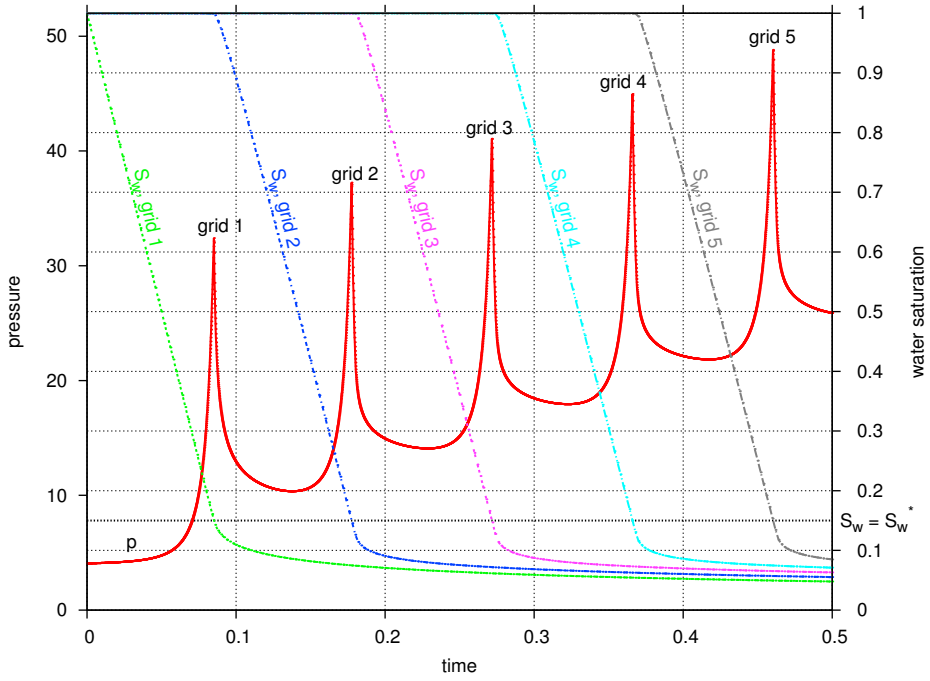

Figure 6: Pressure versus time for $x = 0.15$, compared to the saturation versus time at $x = 0.15$, $x = 0.25$, $x = 0.35$, $x = 0.45$ and $x = 0.55$, for $N = 10$, $M = 1$, $S_w^* = 0.2$, with $u_L = 10$ described on the left boundary and $p_R = 1$ prescribed on the right boundary

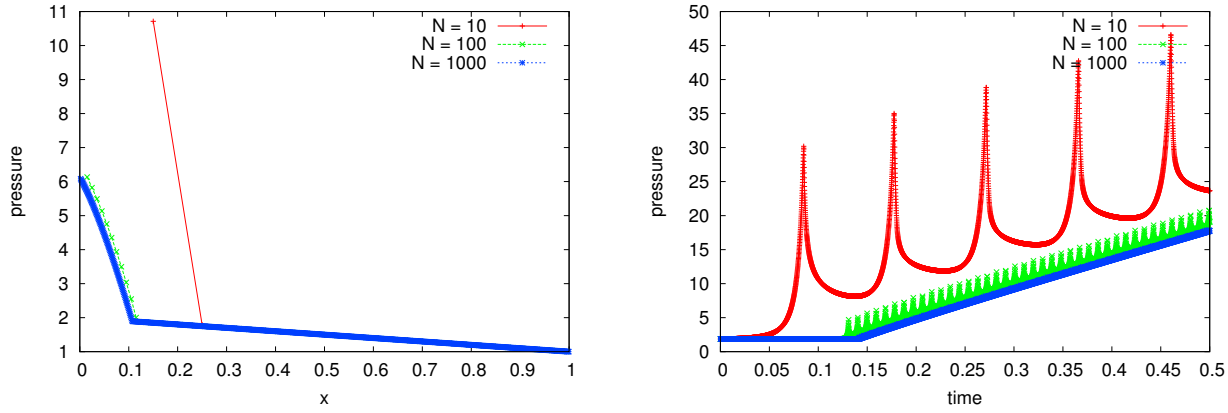

(a) $t = 0.1$ (b) $x = 0.15$

Figure 7: Non-oscillatory solutions in space (left) and oscillatory solutions in time (right) for different grid resolutions and $M = 1$, $S_w^* = 0.15$, $\kappa = 1000$ and $R = 10000$, $u_L = 1$,$p_R = 1$.

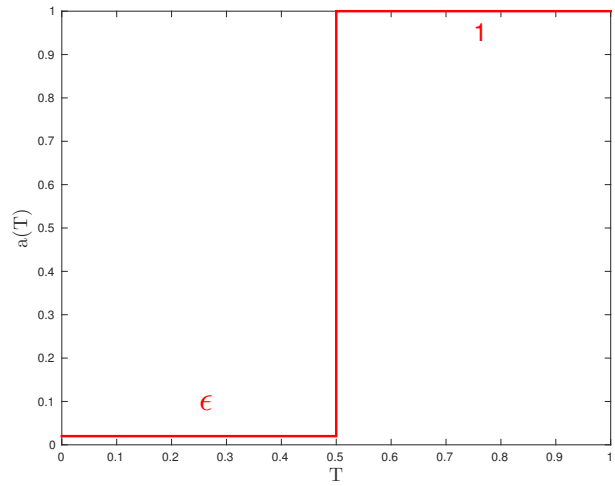

Figure 8 *Discontinuous thermal conductivity $a(T)$ for $T^* = 0.5$ and $\varepsilon = 0.01$.*

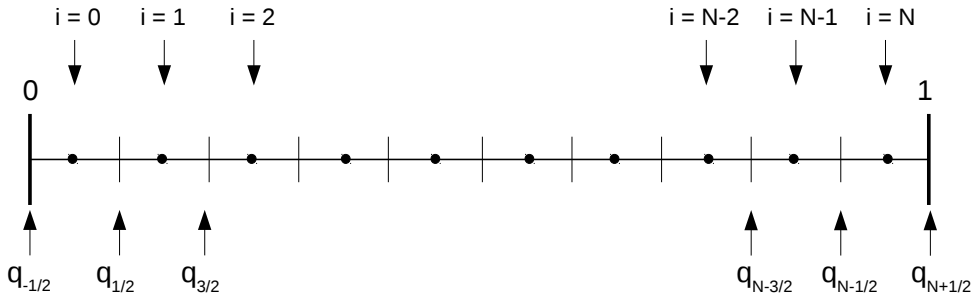

Figure 9 *Numerical grid over the domain $[0, 1]$.*

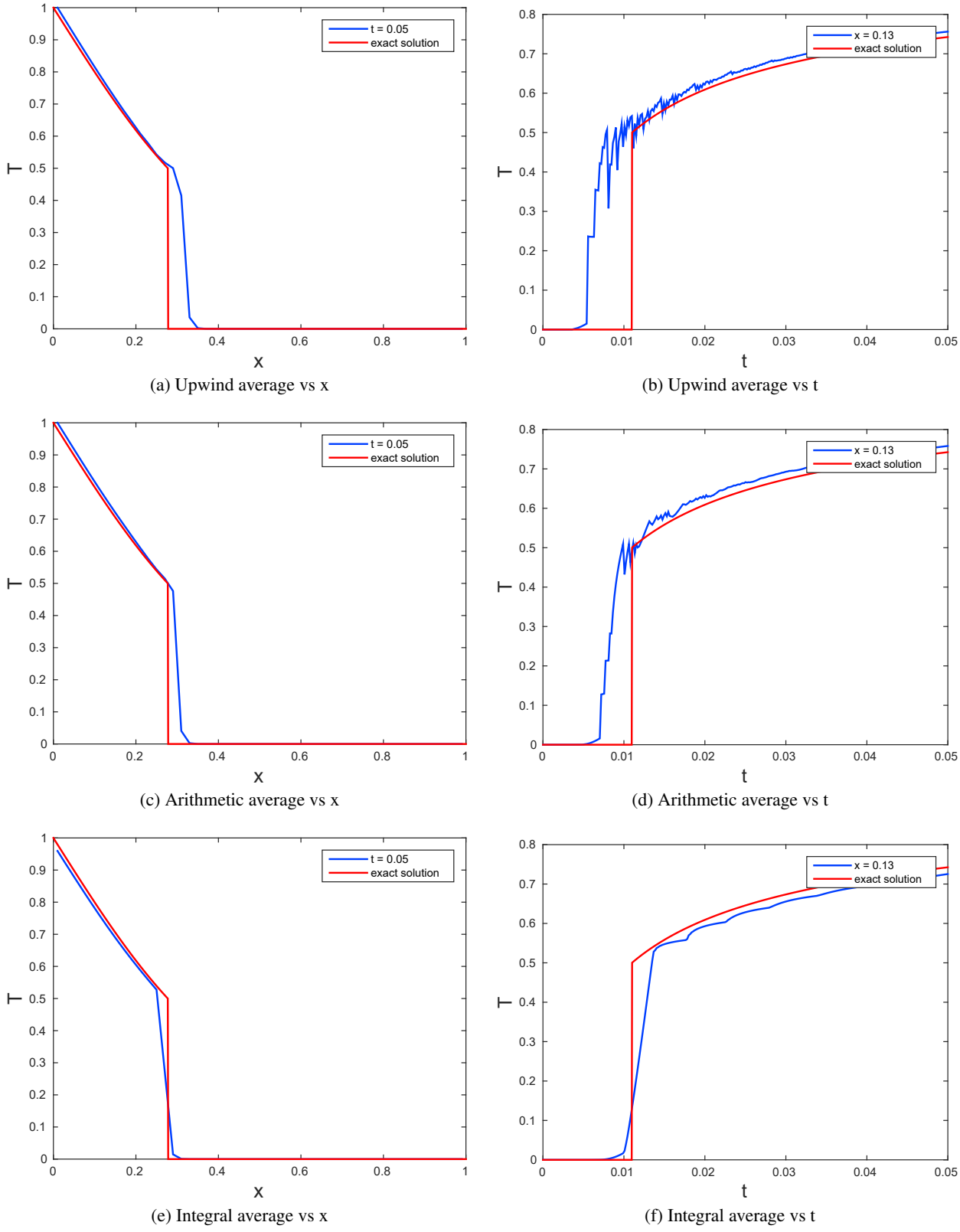

(a) Upwind average vs x

(b) Upwind average vs t

(c) Arithmetic average vs x

(d) Arithmetic average vs t

(e) Integral average vs x

(f) Integral average vs t

Figure 10 *Numerical and analytical temperature profiles of the heat equation with discontinuous conductivity, where* $\Delta x = 0.02$, $\Delta t = 1.8 \cdot 10^{-4}$, $T^* = 0.5$ *and* $\varepsilon = 0.01$.

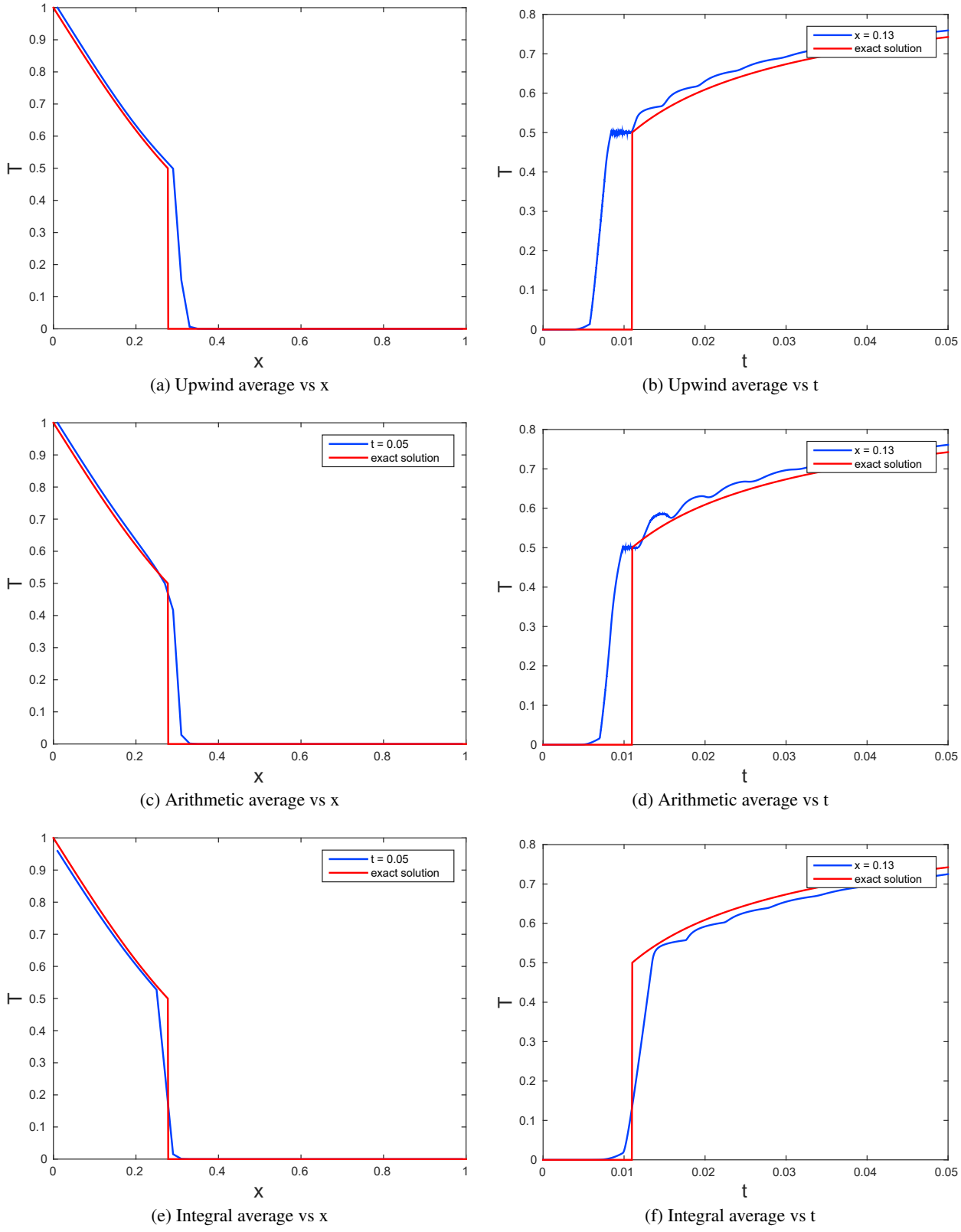

(a) Upwind average vs x

(b) Upwind average vs t

(c) Arithmetic average vs x

(d) Arithmetic average vs t

(e) Integral average vs x

(f) Integral average vs t

Figure 11 *Numerical and analytical temperature profiles of the heat equation with discontinuous conductivity, where* $\Delta x = 0.02$, $\Delta t = 1.8 \cdot 10^{-6}$, $T^* = 0.5$ *and* $\varepsilon = 0.01$.

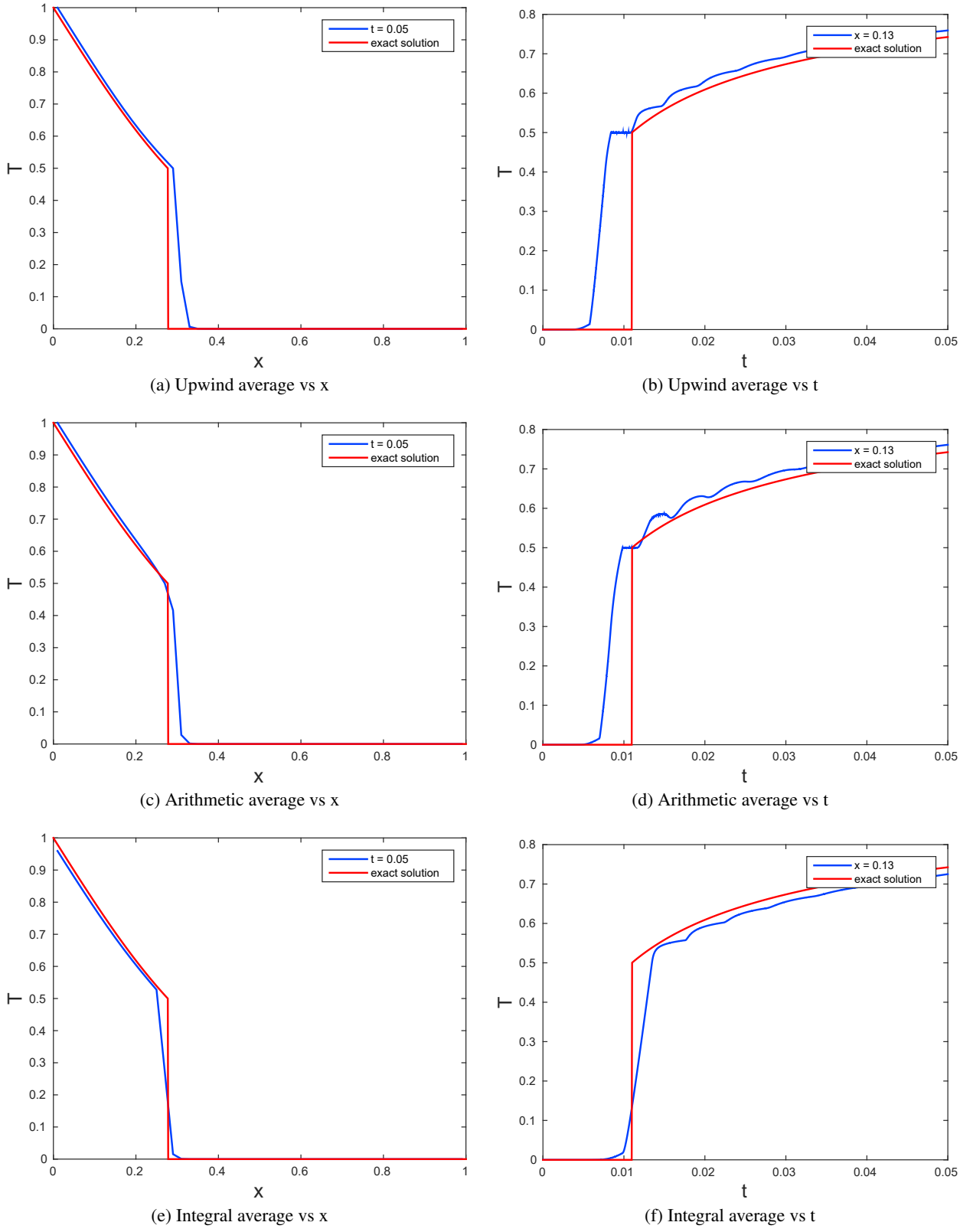

(a) Upwind average vs x

(b) Upwind average vs t

(c) Arithmetic average vs x

(d) Arithmetic average vs t

(e) Integral average vs x

(f) Integral average vs t

Figure 12: Numerical and analytical temperature profiles of the heat equation with discontinuous conductivity, where $\Delta x = 0.02$, $\Delta t = 1.8 \cdot 10^{-7}$, $T^* = 0.5$ and $\varepsilon = 0.01$.

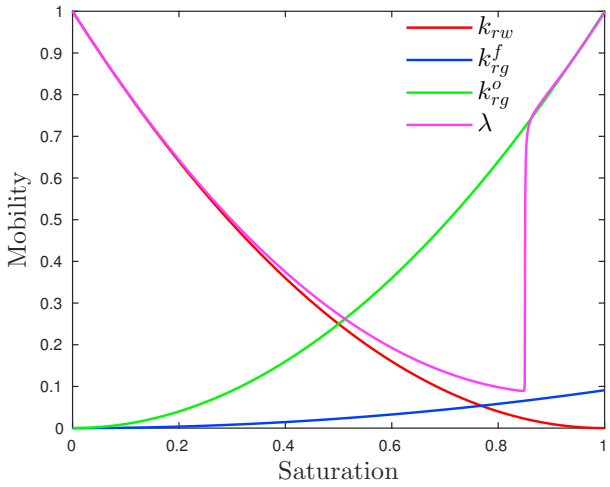

Figure 13: Relative permeability functions of water, gas and foam and the total mobility λ at a fixed time for $M = 1$, $S_w^* = 0.15$.

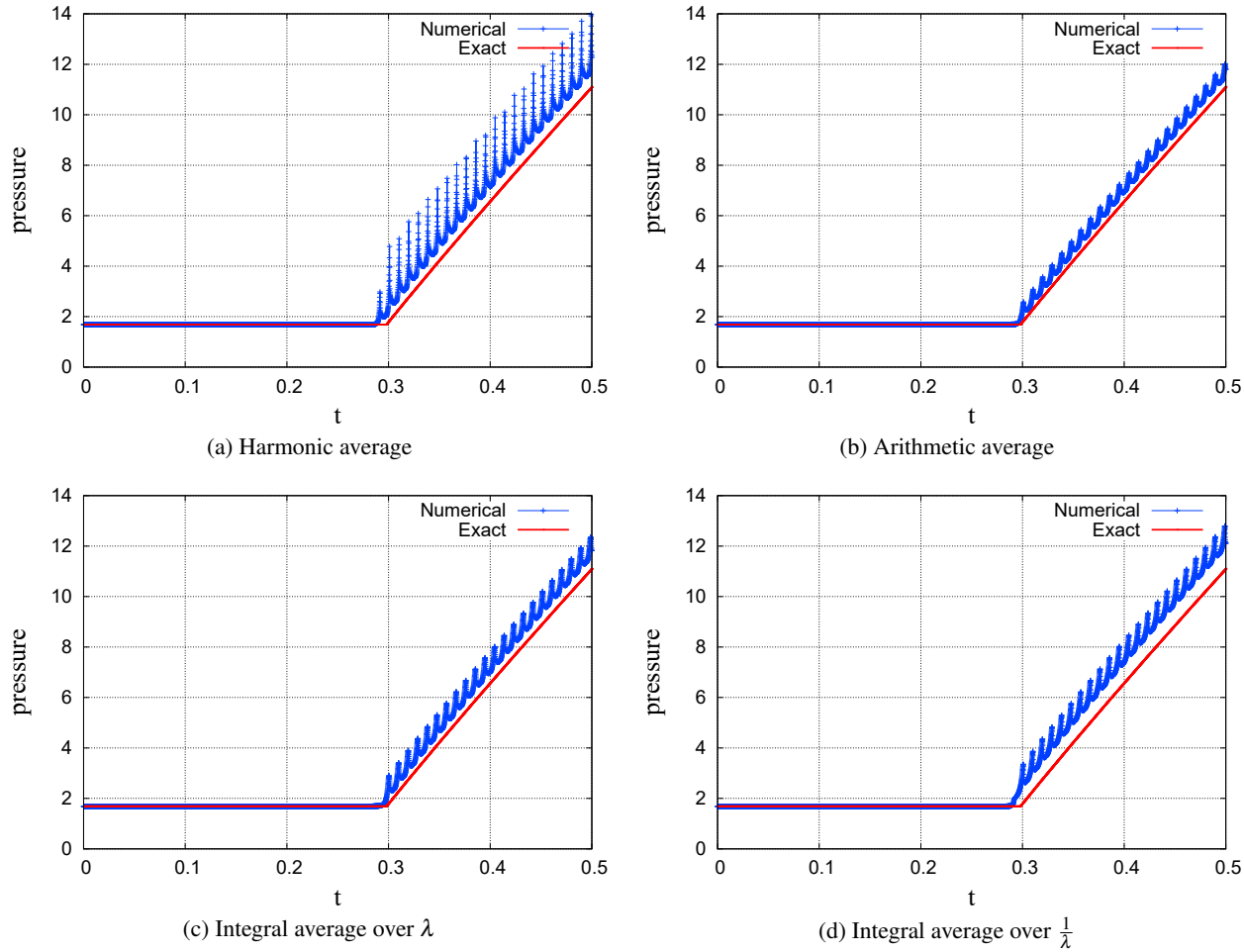

(a) Harmonic average

(b) Arithmetic average

(c) Integral average over λ

(d) Integral average over $\frac{1}{\lambda}$

Figure 14: Pressure vs time $x = 0.15$ for $N = 100$, $M = 1$, $S_w^* = 0.2$, with $u_L = 1$ described on the left boundary and $p_R = 1$ prescribed on the right boundary.

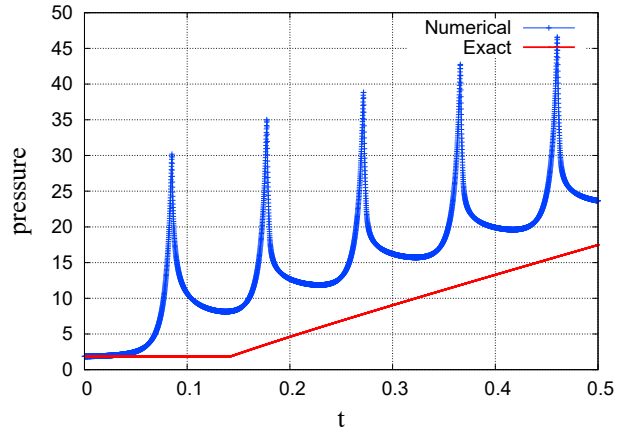

(a) Upwind average

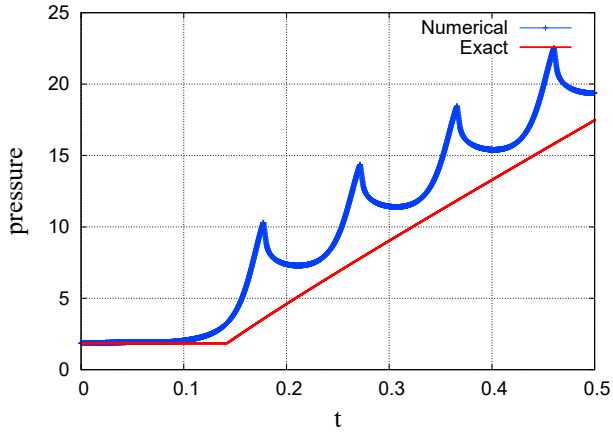

(b) Arithmetic average

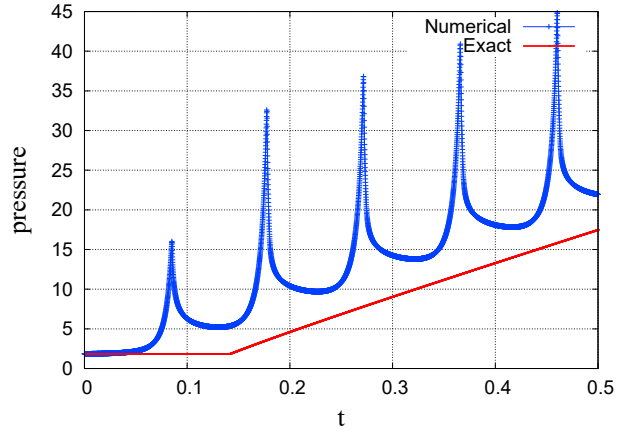

(c) Harmonic average over λ

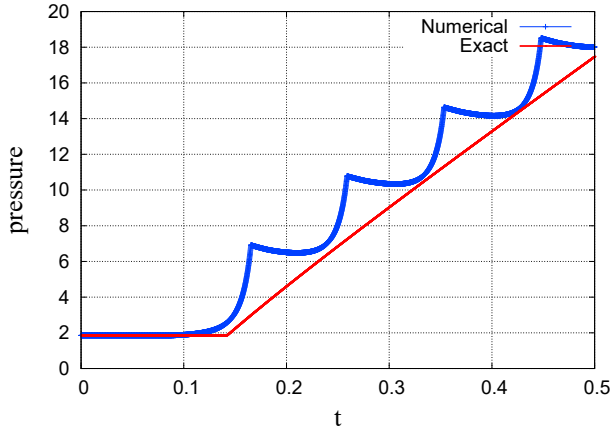

(d) Maximum over $\frac{1}{\lambda}$

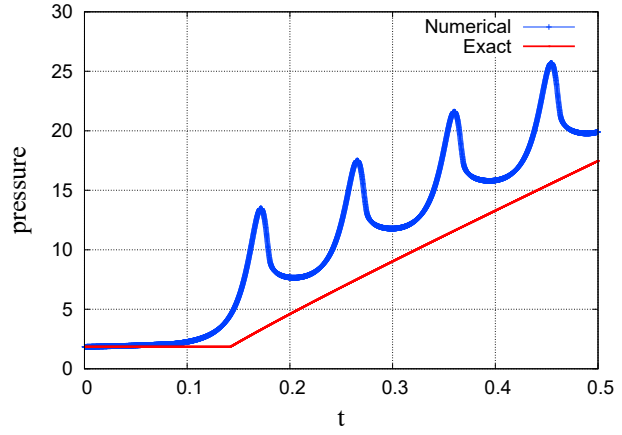

(e) Integral average over λ

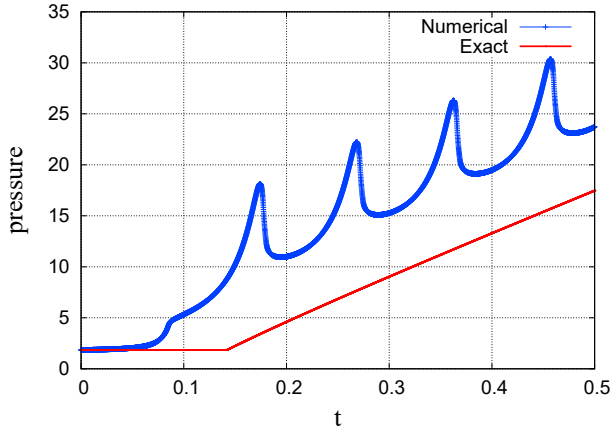

(f) Integral average over $\frac{1}{\lambda}$

Figure 15: Pressure vs time at $x = 0.15$ for $N = 10$, $M = 1$, $S_w^* = 0.2$, with $u_L = 10$ described on the left boundary and $p_R = 1$ prescribed on the right boundary.

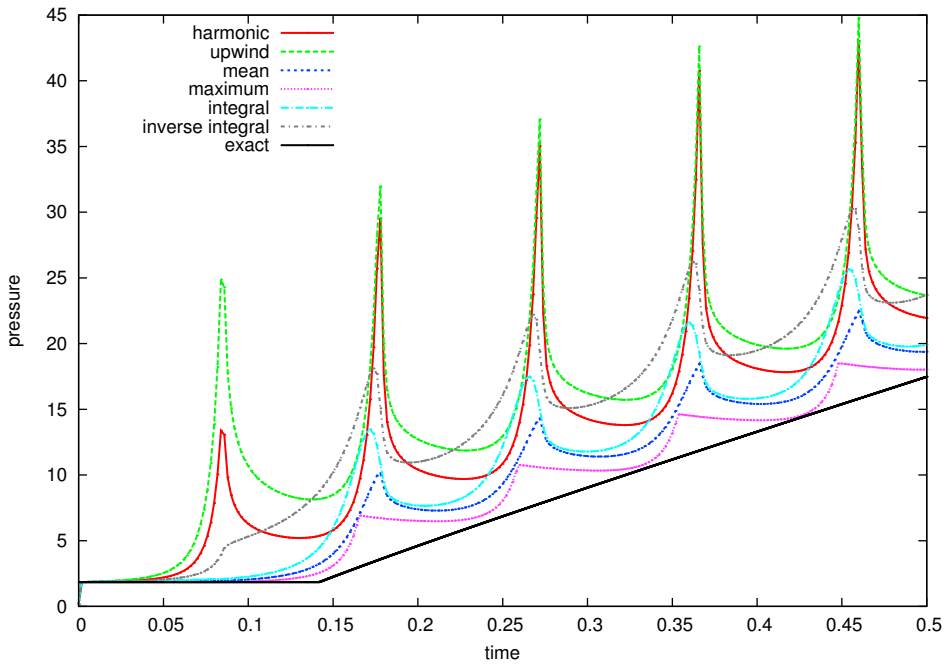

Figure 16: Pressure versus time for $N = 10$, $M = 1$, $S_w^* = 0.2$, with $u_L = 10$ prescribed on the left boundary and $p_R = 1$ prescribed on the right boundary.